Hindawi
Geofluids
Volume 2020, Article ID 8814352, 13 pages
https://doi.org/10.1155/2020/8814352

Research Article

A Crack Propagation Control Study of Directional Hydraulic Fracturing Based on Hydraulic Slotting and a Nonuniform Pore Pressure Field

Yugang Cheng,[1,2,3,4] **Zhaohui Lu**,[2,3] **Xidong Du**,[5] **Xuefu Zhang**,[1] **and Mengru Zeng**[4]

[1]*State Key Laboratory of Mountain Bridge and Tunnel Engineering, Chongqing Jiaotong University, Chongqing 400074, China*
[2]*National and Local Joint Engineering Research Center of Shale Gas Exploration and Development, Chongqing Institute of Geology and Mineral Resources, Chongqing 400042, China*
[3]*Key Laboratory of Shale Gas Exploration, Ministry of Land and Resources, Chongqing Institute of Geology and Mineral Resources, Chongqing 400042, China*
[4]*School of Resources and Safety Engineering, Chongqing University, Chongqing 400030, China*
[5]*State Key Laboratory of Nuclear Resources and Environment, School of Earth Sciences, East China University of Technology, Nanchang, Jiangxi 330013, China*

Correspondence should be addressed to Xidong Du; xidongdu@126.com

Received 27 April 2020; Revised 1 July 2020; Accepted 11 July 2020; Published 3 August 2020

Academic Editor: Mandadige S. A. Perera

Hydraulic fracturing techniques for developing deeply buried coal reservoirs face routine problems related to high initial pressures and limited control over the fracture propagation direction. A novel method of directional hydraulic fracturing (DHF) based on hydraulic slotting in a nonuniform pore pressure field is proposed. A mechanical model is used to address crack initiation and propagation in a nonuniform pore pressure field, where cracks tend to rupture and propagate towards zones of high pore pressure for reducing the effective rock stress more. The crack initiation pressure and propagation morphology are analyzed by rock failure process analysis software. The numerical results show that the directional propagation of hydraulic fracturing cracks is possible when the horizontal stress difference coefficient is less than or equal to 0.5 or the slotting deviation angle is less than or equal to 30°. These findings are in good agreement with experimental results, which support the accuracy and reliability of the proposed method and theory.

1. Introduction

In 2018, the proportion of coal consumption declined to 27.2% in the global primary energy consumption structure while that of natural gas increased to 23.8%. The natural gas market has a strong development momentum, both production and consumption have achieved substantial growth. Efficient exploitation of coalbed methane (CBM), an important unconventional natural gas, is of significant demand for global coal production safety and poses an important strategy for energy structure optimization [1, 2]. China remains one of the world's largest energy consumer, accounting for more than 30% (34%) of the global net increase in energy consumption in 2018. Despite their abundance of about 36.81 trillion m^3, the occurrence conditions of CBM in China are extremely complex, with the prominent characteristics of low permeability and high geostress. Effective stress increases with CBM depth and can lead to restrained gas slippage and compressed coal seam cracks, which reduce coal seam permeability and complicate exploration [3].

With the development of science, engineering technology has gradually become refined in practical application. Hydraulic fracturing was first applied to the petroleum industry and then was subsequently applied to coal mines [4]. Now, it is one of the most effective methods to increase coal seam permeability [5–9]. In theory, the hydraulic

fracture orientation is dictated by and is perpendicular to the minimum in situ stress orientation [10]. However, certain problems controlled by original ground stresses (e.g., high initial pressure, single crack propagation direction) continue to pose practical challenges [11, 12]. In some cases, directional hydraulic fracturing (DHF) is more advantageous and efficient than conventional hydraulic fracturing [13]. For example, the treatment of high mining pressure on a coal seam goaf roof requires DHF to cut the hard rock [14–16]. Coal roadway driving also requires DHF to increase permeability and preextract gas from the coal seam along the preset direction [17, 18]. Initially, scholars used multihole drilling arrangements to relieve the stresses in a certain direction within the coal seam, while at the same time, controlling the expansion direction of hydraulic fracture [19]. Subsequently, some scholars put forward prefabricated artificial cracks in the coal seam to influence the hydraulic cracks based on the effect of hydraulic slotting [20, 21]. Then, DHF is gradually used to prevent rockburst or increase the permeability directionally in underground coal mining as a combination of hydraulic fracturing and multihole drilling or hydraulic slotting [17, 22, 23]. Compared with multihole drilling, hydraulic slotting offers improved control over the direction range of crack propagation from a single borehole. DHF experiments were first explored by Mizuta et al. but did not address how to expand fractures in a desired direction [24]. Yan et al. showed that certain hydraulic slotting arrangements can improve fracture control, which have been verified by gas field extraction experiments [22]. However, the variation of in situ stress and the angle of the maximum horizontal principal stress to the direction of hydraulic slot layout were not considered, both of which are critical to crack propagation and deflection [25]. Physical experiments and numerical analysis have also been used to investigate the relationship of a single hydraulic slot and its initial pressure and crack propagation behavior [26, 27], while practical applications must consider interactions between multiple drilling holes or slots. Although many scholars have made great breakthroughs in the method of DHF, the conditions under which the directional crack propagation can be controlled therefore remain poorly understood, in addition to the DHF crack propagation mechanism.

In this study, a new DHF method is proposed based on the integration of hydraulic slotting and a nonuniform pore water pressure gradient. We have designed a mechanical model that demonstrates the guiding control mechanism of hydraulic fracturing using a nonuniform pore water pressure gradient. Numerical analysis is used to constrain the relationship between the DHF crack propagation direction and two key parameters: (1) the coefficient of horizontal stress difference and (2) the angle between the hydraulic slotting and direction of maximum horizontal principal stress. The results are compared with physical experiments.

2. DHF Methodology and Inducing Theory by a Nonuniform Pore Water Pressure Gradient

2.1. DHF Methodology. The technical principles of crack propagation control using the DHF methods proposed in this paper are shown in Figure 1. Hydraulic slotting is first used to form an orderly and consistent groove layout in the coal seam. Stable water pressure is then maintained in the slotting borehole prior to fracturing to form a nonuniform pore pressure gradient field. Hydraulic fracturing is then implemented, and hydraulic cracks are obtained in the desired direction.

DHF methods based on the integration of hydraulic slotting and nonuniform pore water pressure gradient show strategic advantages over conventional hydraulic fracturing. For example, the original stress field surrounding the slot can be redistributed with the aid of a water jet. A DHF zone is built where the maximum principal stress exceeds the original stress, and the direction of the former is then deflected from the original horizontal orientation into the slotting direction. The original in situ stress can thus be overcome, and control of the fracturing crack propagation direction can be obtained [28, 29]. Another advantage of this approach is that a nonuniform pore pressure gradient can form in the coal mass upon the injection of water in different boreholes, which reduces the effective stress and energy required for crack expansion [30]. AlTammar et. al have proved that hydraulic fracture trajectories and fracturing pressures can be significantly affected by injection-induced stress through an experimental study [31]. Therefore, a theoretical analysis of the effect of pore pressure field on fracture initiation and propagation pressure was studied in this study.

The proposed method combines hydraulic slotting with a nonuniform pore pressure gradient to expand hydraulic fracturing cracks and transform in situ stress. Reasonable borehole arrangement, hydraulic slotting, water injection, hydraulic fracturing, and other steps, as described in the following sections, can improve hydraulic crack initiation, expand crack extension, and meet engineering requirements regarding the orientation or specified location of propagated cracks to increase coal seam permeability.

The transformation of a coal body's stress field by hydraulic slotting has been described in detail in literature and is not included here [18]. The following section is a theoretical explanation of the effects of nonuniform pore pressure gradient on the initiation and fracture propagation pressures.

2.2. Effects of a Nonuniform Pore Pressure Gradient on the Directional Crack Propagation Mechanism

2.2.1. Effect of Nonuniform Pore Water Pressure on the Fracture Initiation Pressure. The stress state of a borehole perpendicular to a coal seam is shown in Figure 2. A guiding borehole is set near the hydraulic fracturing borehole to study the effect of a nonuniform pore pressure gradient. High-pressure water is injected into the guiding borehole to form a nonuniform pore pressure gradient in the coal seam, which affects the stress of the hydraulic fracturing borehole.

When the effect of a nonuniform pore water pressure gradient is not taken into account, the stress state of the fracturing borehole wall can be expressed as Equation (1) [32–34]. The stress state of the fracturing borehole wall in Equation

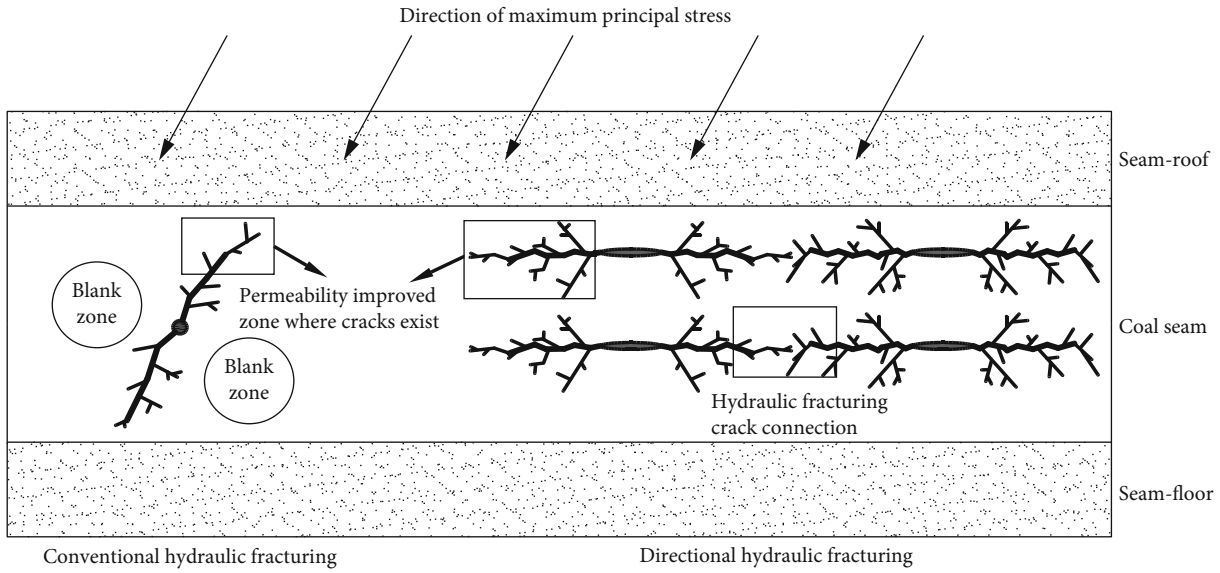

Figure 1: Schematic diagram of directional hydraulic fracturing (DHF) based on hydraulic slotting and a nonuniform pore pressure gradient.

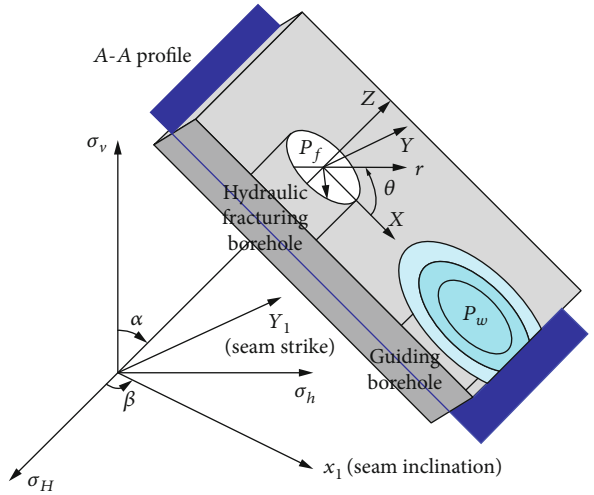

Figure 2: Stress state of a borehole under a nonuniform pore pressure gradient.

(1) was calculated in the cylindrical coordinate of (X, Y, Z), which was transferred from the coordinate of in situ rock stress $(\sigma_H, \sigma_h, \sigma_v)$ [35].

$$\begin{cases} \sigma_r = p_f, \\ \sigma_\theta = (\sigma_x + \sigma_y) - 2(\sigma_x - \sigma_y)\cos 2\theta - 4\tau_{xy}\sin 2\theta - p_f, \\ \sigma_{zz} = \sigma_z - \nu[2(\sigma_x + \sigma_y)\cos 2\theta + 4\tau_{xy}\sin 2\theta], \\ \tau_{\theta z} = 2\tau_{yz}\cos\theta - 2\tau_{xz}\sin\theta, \\ \tau_{r\theta} = \tau_{zr} = 0, \end{cases} \quad (1)$$

where σ_v is the vertical principal stress, σ_H and σ_h are the maximum and minimum horizontal principal stresses in the coordinate of in situ rock stress, respectively, p_f is the water pressure in the hydraulic fracturing borehole, and σ_r, σ_θ, σ_{zz}, $\tau_{r\theta}$, $\tau_{\theta z}$, and τ_{zr} are the radial, tangential, and axial components of the normal and shear stresses at the hydraulic fracturing borehole wall inclined at an angle of θ with σ_y, respectively.

Figure 2 shows a coal seam that is cut along the A-A plane, and the stress variation of the fracturing borehole wall is shown in Figure 3. The guiding borehole is assumed to maintain a stable injection of high-pressure water in the coal seam reservoir with an influence range R. According to the thick-wall planar radial flow theory, the pressure distribution equation and boundary conditions at a distance d from the guiding borehole can be written as

$$\begin{cases} \dfrac{d}{dd}\left(d\dfrac{dp}{dd}\right) = 0, (r_w \le d \le R), \\ p(d = r_w) = p_w, \\ p(d = R) = p_o, \end{cases} \quad (2)$$

where r_w is the radius of the guiding borehole, p_w is the control water pressure in the guiding borehole, and p_o is the original pore water pressure of the coal seam. The pore pressure variation within R of the guiding borehole can be obtained as

$$p' = p_w - \frac{p_w - p_o}{\ln(R/r_w)} \ln\frac{d}{r_w}. \quad (3)$$

According to the principle of effective stress, stresses change in the vicinity of the hydraulic borehole within R. Since the pore water pressure only affects the normal stress,

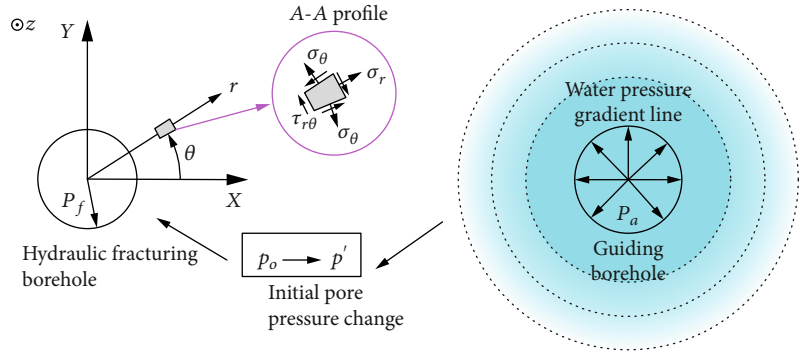

Figure 3: The formation of nonuniform pore pressure field and its influence on fracturing borehole stress.

it has no effect on the shear stress. The normal stress in Equation (1) can therefore be rewritten as

$$\begin{cases} \bar{\sigma}_x = \sigma_x - p', \\ \bar{\sigma}_y = \sigma_y - p'. \end{cases} \tag{4}$$

Fluid loss can occur at the fracturing borehole wall due to differences between the water pressure in the fracturing borehole and the pore pressure of the coal seam, which cause variation of the stress surrounding the borehole. According to the thermoelastic stress solution for a thick-walled cylinder, the change of tangential stress on the wall can be obtained as

$$\Delta\sigma_\theta = \left(p_f - p'\right)\varphi\frac{1-2\nu}{1-\nu}, \tag{5}$$

where φ is the Biot constant of the coal seam and ν is Poisson's ratio. The tangential stress is therefore modified to

$$\sigma_\theta{}' = \sigma_\theta + \Delta\sigma_\theta. \tag{6}$$

When the wall of the pressure-cracked hole is damaged,

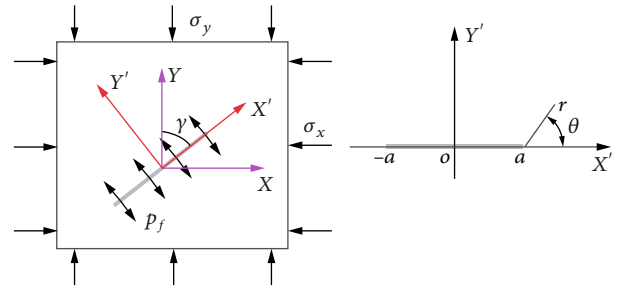

Figure 4: Stress state of a propagating crack.

Equation (6) should be met according to the maximum tensile strength failure criterion of the borehole wall:

$$\left|\sigma_\theta{}'\right| \geq Rt, \tag{7}$$

where Rt is the tensile strength of rock around the borehole wall.

In the presence of a nonuniform pore water pressure gradient, the critical fracture initiation pressure of the fracturing borehole can be expressed as

$$p_f = \frac{\sigma_x + \sigma_y - 2\left(\sigma_x - \sigma_y\right)\cos 2\theta - 4\tau_{xy}\sin 2\theta + Rt - \left(\varphi\left((1-2\nu)/(1-\nu)\right) + 2\right)\left(p_w - \left((p_w - p_o)/(\ln\left(R/r_w\right))\right)\ln\left(d/r_w\right)\right)}{1 - \varphi\left((1-2\nu)/(1-\nu)\right)}. \tag{8}$$

Poisson's ratio of rock material is always less than 0.5, such that $\varphi\left((1-2\nu)/(1-\nu)\right) + 2 > 0$. When high-pressure water is injected into the guiding borehole, p' is higher than p_o. Assuming that other parameters remain constant, the pore water pressure gradient field formed by the guiding borehole will reduce the initial fracture pressure of the hydraulic fracturing borehole, that is, the borehole will preferentially crack in the direction of the directional borehole because it is the region where the pore pressure has a higher increase.

2.2.2. Effect of Nonuniform Pore Water Pressure on Crack Propagation Pressure. A crack propagated in a fracturing borehole is affected by the nonuniform pore pressure gradient. The following is an analysis of the extended crack pressure. The stress state of a propagating crack of arbitrary width is shown in Figure 4.

By transforming the xoy coordinate system in Figure 4 into the crack coordinate system $x'oy'$, the stress state of the crack affected by in situ stress can be obtained as

$$\begin{cases} \sigma_x{}' = -\left(\sigma_x \sin^2\gamma + \sigma_y \cos^2\gamma\right), \\ \sigma_y{}' = -\left(\sigma_x \cos^2\gamma + \sigma_y \sin^2\gamma\right), \\ \tau_{xy} = \left(\sigma_x - \sigma_y\right)\sin\gamma\cos\gamma. \end{cases} \tag{9}$$

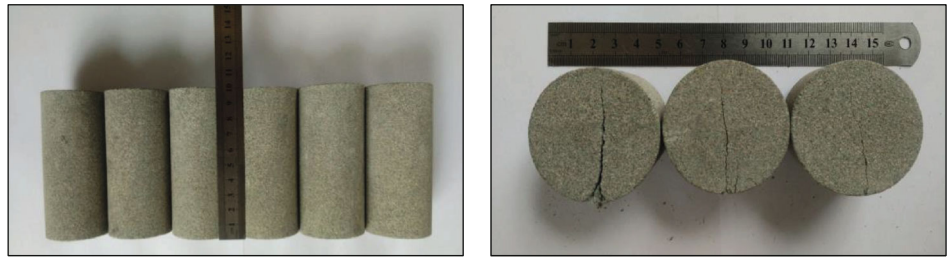

(a) (b)

Figure 5: Uniaxial compression test specimen and failure results.

Table 1: Physical and mechanical properties of sandstone used in the numerical model.

Category	Density (kg/m^3)	Tensile strength (MPa)	Compressive strength (MPa)	Poisson's ratio	Elastic modulus (GPa)
Sandstone	2333	4.09	56.4 MPa	0.24	36 GPa

Previous studies have often characterized rock mass under a complex stress state as a I-II composite. Here, pure type II cracks are not treated under strong compressional shear action. When the effects of the induced pore are ignored, the circumferential tensile strain of a I-II composite crack of length 2a (Figure 4) is obtained as

$$\varepsilon_\theta = \frac{1}{2E\sqrt{2\pi r}}\left[\begin{array}{c} K_{\mathrm{I}} \cos\dfrac{\theta}{2}(1-3\nu+\cos\theta+\nu\cos\theta) - \\ K_{\mathrm{II}}\left(3\cos\dfrac{\theta}{2}\sin\theta+3\nu\sin\dfrac{\theta}{2}\cos\theta-\nu\sin\dfrac{\theta}{2}\right)\end{array}\right], \tag{10}$$

where K_{I} and K_{II} are the stress intensity factors of type I and type II cracks, respectively, and the stress intensity factor in Equation (10) is given as

$$\begin{cases} K_{\mathrm{I}} = \left[p_f - \left(\sigma_x \sin^2\gamma + \sigma_y \cos^2\gamma\right)\right]\sqrt{\pi a}, \\ K_{\mathrm{II}} = \left(\sigma_x - \sigma_y\right)\sin\gamma\cos\gamma\sqrt{\pi a}. \end{cases} K_{\mathrm{I}} > 0, \tag{11}$$

According to maximum circumferential tensile strain theory, a crack expands when ε_θ reaches the critical value ε_e, namely:

$$\varepsilon_\theta = \varepsilon_e. \tag{12}$$

Such that the water pressure in the propagated crack can be obtained as

$$\begin{aligned} p_f = {} & \frac{2E\varepsilon_e\sqrt{2r} + B\sin\gamma\cos\gamma\sqrt{a}\left(\sigma_x-\sigma_y\right)}{A\cos(\theta/2)\sqrt{a}} + \sigma_x\sin^2\gamma \\ & + \sigma_y\cos^2\gamma - \left(p_w - \frac{p_w - p_o}{\ln(R/r_w)}\ln\frac{d}{r_w}\right), \end{aligned} \tag{13}$$

where $A = 1 - 3\nu + \cos\theta + \nu\cos\theta$ and $B = 3\cos(\theta/2)\sin\theta + 3\nu\sin(\theta/2)\cos\theta - \nu\sin(\theta/2)$.

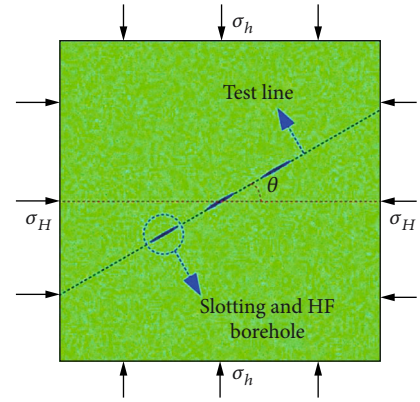

Figure 6: Model design in the numerical analysis: θ represents the slotting deviation angle.

A comparison of Equations (8) and (13) shows that the effect of a nonuniform pore water pressure gradient formed by the guiding borehole on the crack propagation pressure is consistent with the crack initiation pressure. Due to the self-organizing behavior of crack propagation, the crack will expand in the direction of the lowest propagation pressure to reduce the energy required for expansion. The formation of a nonuniform pore water pressure gradient can therefore effectively induce crack propagation. It is worth noting that higher water pressure in the guiding borehole and a closer distance from the hydraulic fracturing borehole both lead to stronger crack initiation and propagation-induced effects by the guiding borehole.

3. Numerical Analysis of DHF Crack Morphology

The coupled analysis of flow and solid mechanics in rock failure process analysis software (RFPA^{2D}-Flow) was used to study initial pressure and DHF crack propagation [36, 37]. The RFPA^{2D}-Flow was developed by Dalian Mechanics Software Co. Ltd. (China), which was designed to simulate the fracture and failure processes of quasibrittle materials

Table 2: Loading cases considered in the numerical analysis.

Load cases	Maximum horizontal stress σ_H (MPa)	Minimum horizontal stress σ_h (MPa)	Horizontal stress difference coefficient K_h	Slotting deviation angle θ (°)
1#	4.5	3	0.5	15°
2#	5.25	3	0.75	15°
3#	6	3	1	15°
4#	6.75	3	1.25	15°
5#	4.5	3	0.5	30°
6#	5.25	3	0.75	30°
7#	6	3	1	30°
8#	6.75	3	1.25	30°
9#	4.5	3	0.5	45°
10#	5.25	3	0.75	45°
11#	6	3	1	45°
12#	6.75	3	1.25	45°
13#	4.5	3	0.5	60°
14#	5.25	3	0.75	60°
15#	6	3	1	60°
16#	6.75	3	1.25	60°
17#	4.5	3	0.5	75°
18#	5.25	3	0.75	75°
19#	6	3	1	75°
20#	6.75	3	1.25	75°
21#	4.5	3	0.5	90°
22#	5.25	3	0.75	90°
23#	6	3	1	90°
24#	6.75	3	1.25	90°

[22]. The rock in RFPA^{2D}-Flow was assumed as a brittle elastic material with residual strength, and its loading and unloading behaviors were in accordance with elastic damage mechanics. In addition, the fluid flow in rock follows Biot's theory.

3.1. Material Parameters. The authors have published relevant physical simulation experiments using sandstones in order to avoid the effects of excessive coal-derived native joints or cracks on the guiding cracks. The sandstones were taken from the Songzao coal mine area in Chongqing, China. The results can be found in the references [17, 18]. To facilitate comparison, the numerical simulation parameters used in this paper are also consistent with the physical simulation experiment. Figure 5 shows a Φ50mm × 100 mm standard cylindrical uniaxial compression test specimen made of sandstone and results after failure in the previous physical simulation experiment. The basic mechanical parameters of sandstone used in the model are listed in Table 1.

3.2. Numerical Model Procedure. The model design and stress loading method are shown in Figure 6. The model size is 300 × 300 mm, and the grid is divided into a total of 3.2×10^5 sections. The horizontal direction of the model is loaded with the maximum horizontal principal stress. Three hydraulic slots are arranged in a straight line, and all slots would be injected with water pressure as hydraulic fracturing boreholes simultaneously. The slots are oval with axes of 3 and 30 mm, and the spacing between each slot is 30 mm. The initial water injection pressure inside each slot was set to 2 MPa with a 0.1 MPa increase in each following step size. Loading stopped upon the stabilization of propagated crack morphology.

Previous studies have shown that the most important factors affecting DHF crack propagation are the difference between horizontal stresses and the angle between the maximum principal stress and the slotting direction [25, 38], hereinafter referred to as the slotting deviation angle. In this study, the horizontal stress difference coefficient is used to reflect the horizontal principal stress difference during loading. The horizontal stress difference coefficient is calculated by

$$K_h = \frac{\sigma_H - \sigma_h}{\sigma_h}. \tag{14}$$

The depth of China's CBM development is generally 400-1000 m, and the horizontal stress difference coefficient in this range is generally 0.4-1.2. The slotting

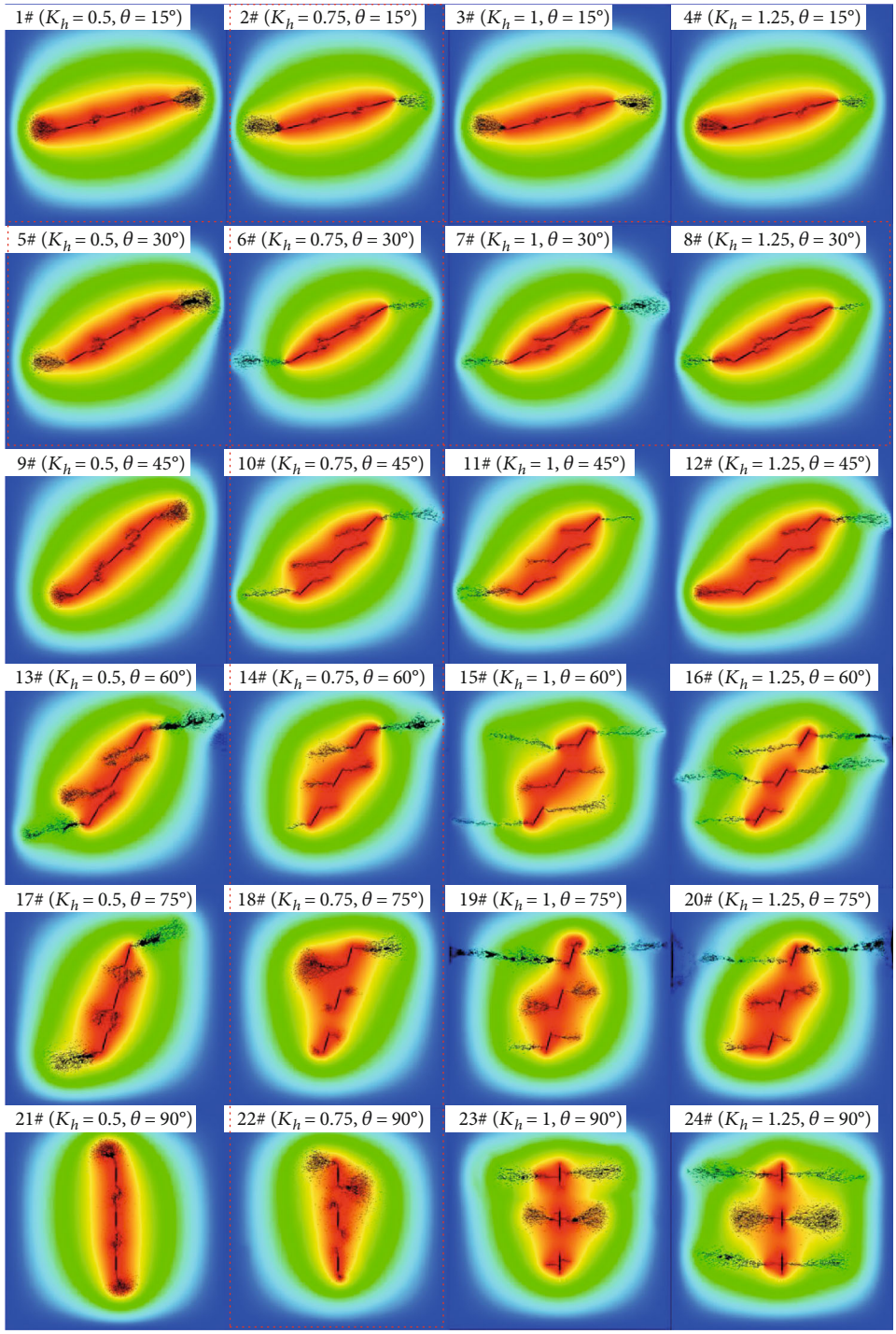

Figure 7: Crack propagation morphology of the 24 numerical model simulations.

deviation angle is 0° when the hydraulic slotting direction is parallel to the maximum horizontal principal stress direction and 90° when the directions are perpendicular to one another.

We designed 24 model sets with four horizontal stress difference coefficient values (0.5, 0.75, 1.0, and 1.25) and five slotting deviation angles (15°, 30°, 45°, 60°, 75°, and 90°). The model design number and specific stress loading sizes are listed in Table 2.

4. Numerical Results and Discussion

4.1. DHF Crack Propagation Morphology. The crack propagation morphology of 24 numerical model simulations was analyzed after extension to investigate how the horizontal stress difference coefficient and slotting deviation angle affect DHF, as shown in Figure 7. Two representative crack propagation groups are selected for comparison. The first group includes model numbers 5-8 with a fixed slotting deviation

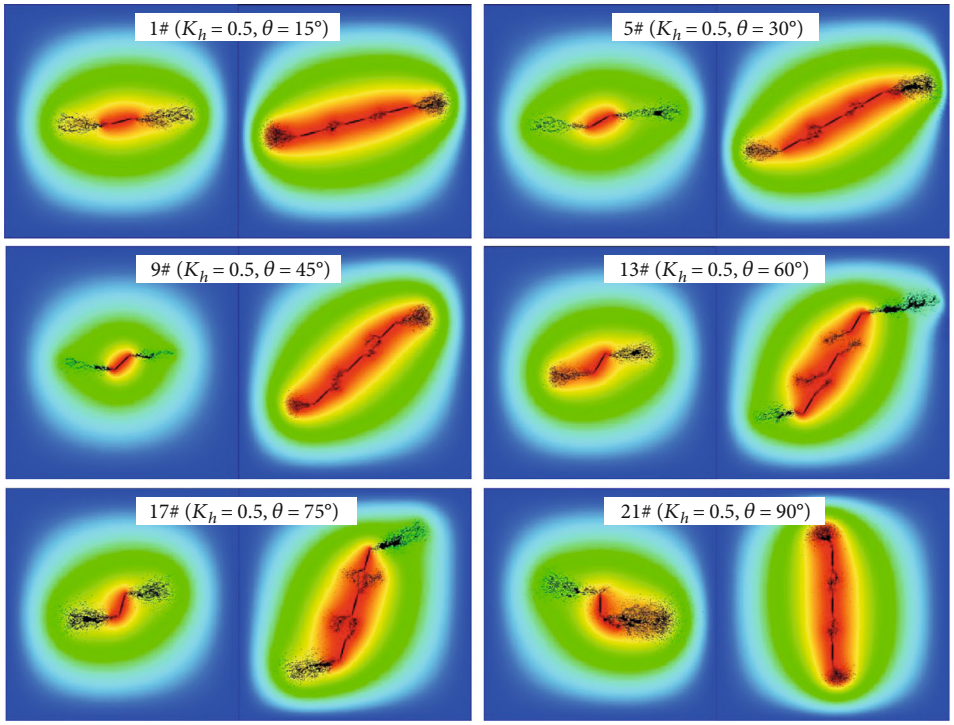

Figure 8: Crack propagation compared with a control group of simulations.

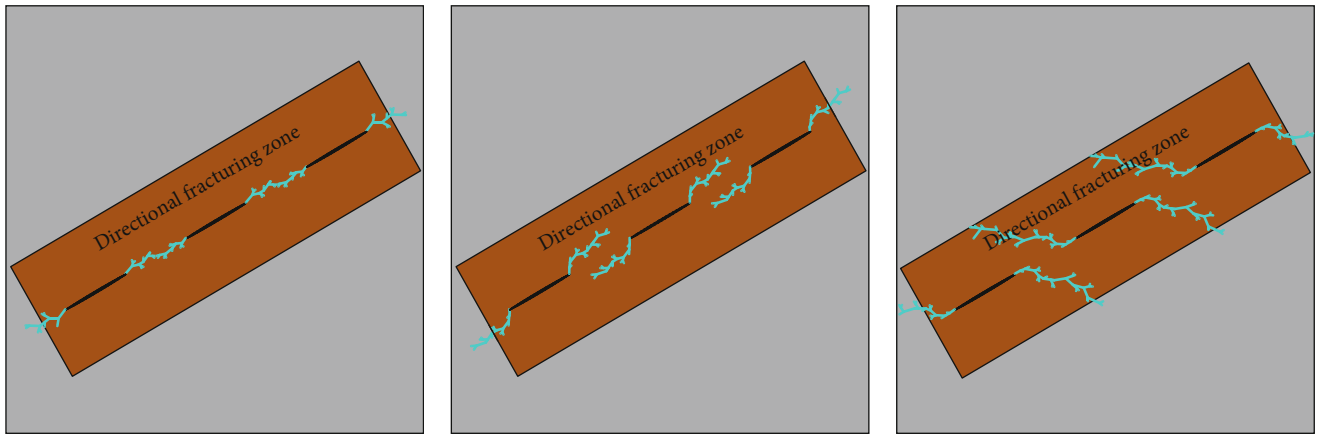

(a) The first crack propagation morphology (b) The second crack propagation morphology (c) The third crack propagation morphology

Figure 9: Three types of directional hydraulic fracturing (DHF) crack propagation morphology.

angle of 30°. As the horizontal stress difference coefficient increases from 0.5 to 1.25, the cracks start to propagate directly in the hydraulic fracturing zone and gradually spread outwards. The second group contains model numbers 2, 6, 10, 14, 18, and 22 with a fixed horizontal stress difference coefficient of 0.75. As the slotting deviation angle increases from 15° to 90°, the cracks gradually propagate out of the directional hydraulic fracturing zone. These findings indicate that larger horizontal stress difference coefficients and slotting deviation angles tend to produce a more unfavorable deviation of the cracks outside of the DHF induction zone.

To better illustrate the feasibility of the DHF method, we performed a control group of simulations. All the models in the first column of Figure 7 capable of DHF were selected, namely, models 1#, 5#, 9#, 13#, 17#, and 21#, for comparison, which the slotting deviation angle varies from 15° to 90° with a fixed horizontal stress difference coefficient of 0.5. The central slotting and HF borehole are preserved in the numerical model that means the stress field and pore water pressure gradient field between adjacent slots are not considered to induce crack propagation. The comparison results are shown in Figure 8. It can be seen that when there is no other slot near a slot, the hydraulic crack may initially rupture and

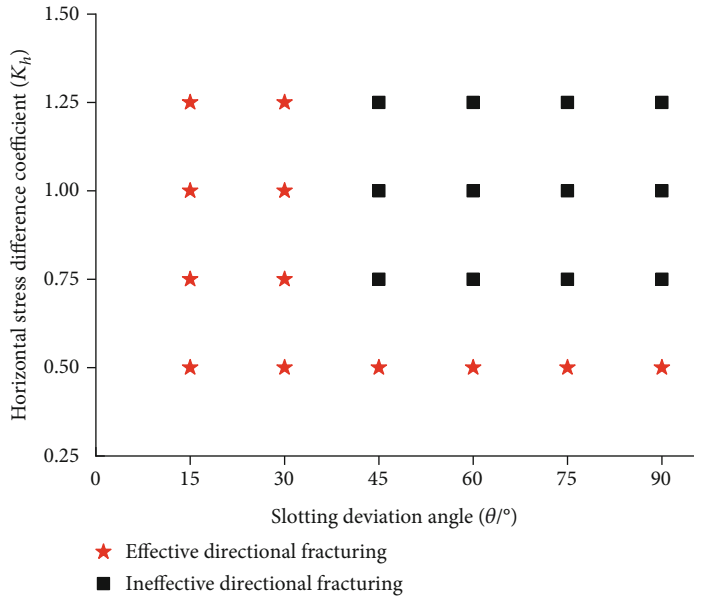

Figure 10: Effective directional fracturing results obtained from the 24 models.

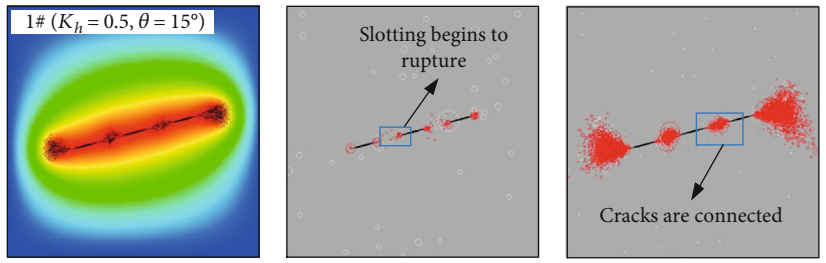

Figure 11: Acoustic emission events of model #1 during fracturing.

expand along the hydraulic slotting due to a certain angle of the slot. However, the maximum horizontal stress controls the direction of crack propagation rapidly. This means a single hydraulic slotting is insufficient to achieve DHF but requires interaction between a series of slots.

In addition, we separate the crack propagation results into three classification types based on morphology, as shown in Figure 9. The first crack propagation type includes direct (i.e., parallel) propagation in the DHF zone, demonstrating the best induction effects. Although the second crack pattern shows indirect crack propagation, the orientation is mostly parallel to the DHF inducing zone. The third crack type does not show a clear effect of the guiding borehole, and cracks tend to propagate along the direction of initial maximum principal stress. It is worth noting that a crack is still mainly controlled by the *in situ* stresses after propagating through the DHF inducing zone and steered to expand along the direction of maximum principal stress.

The crack propagation morphology results obtained from the 24 model simulations were statistically analyzed based on the classifications described above. The first two crack morphology types are regarded as effective directional fracturing, as shown in Figure 10. It can be seen that DHF cracks only propagate directionally when the slotting deviation angle is less than or equal to 30° or the horizontal stress difference coefficient is less than or equal to 0.5. Cracks that form under other conditions are still mostly affected by the initial maximum principal stress.

4.2. Acoustic Emission Events and Initial Pressure Assessment. We used acoustic emission (AE) images to determine and compare the cracking pressure from each model run. Figure 11 shows how the AE pattern changes during the fracturing process of model 1# with a slotting deviation angle of 15° and a horizontal stress difference coefficient of 0.5. The red and white circles in the figure represent the AE energy generated by tensile and compressive stress, respectively. The circle diameter represents the AE energy magnitude, and the number of circles shows the number of AE events. Figure 11(b) shows some typical tensile damage AE events at the slot tip, which represents the rupture onset. We consider the water injection pressure at this step to be the cracking pressure.

4.3. Comparative Analysis of Crack Initiation Pressure and Propagation Morphology with Experimental Results. We have

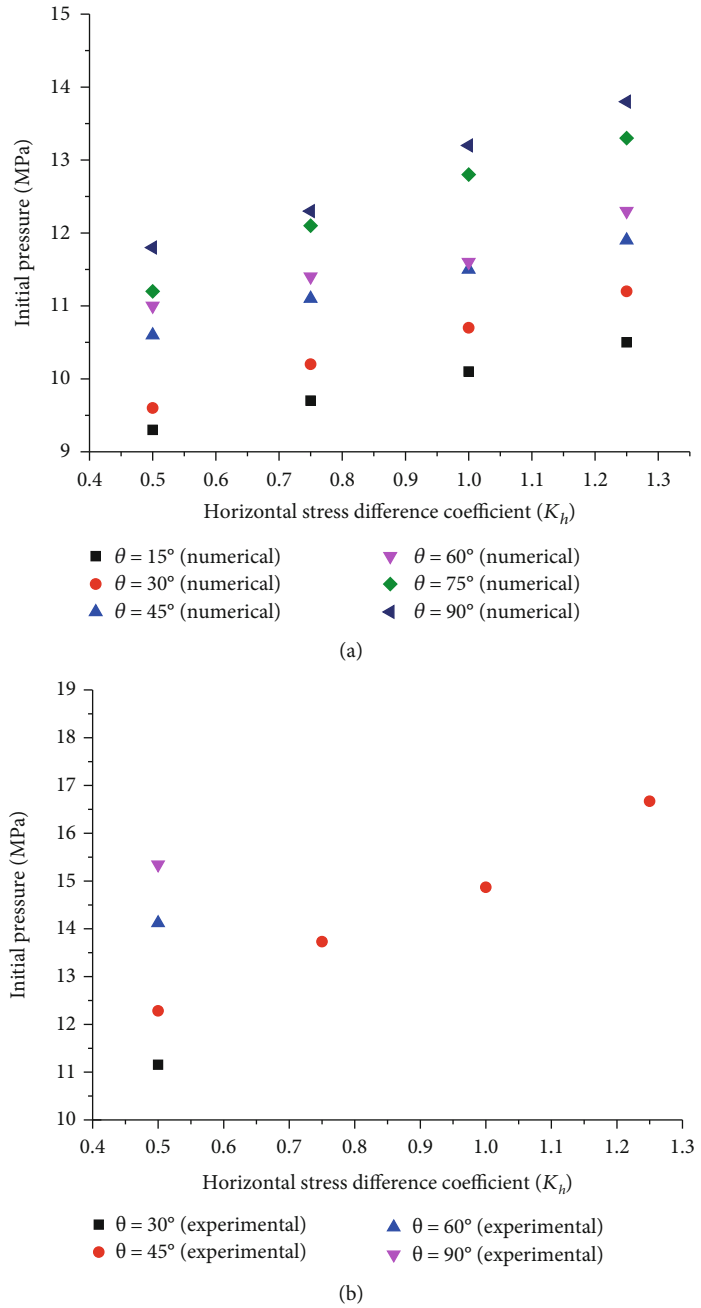

Figure 12: Variation of initial pressure under different conditions from (a) numerical calculation results and (b) physical experimental results [18].

previously reported results from similar and relevant physical DHF experiments. However, the experiments involved the filling of only the central slot with water, while the numerical calculations presented here involve the simultaneous injection of three slots with water and the effect of pore water pressure gradient is considered. Nevertheless, a comparison with experimental data is important for checking the validity of the numerical results.

The fracture initiation pressure of all model simulations (Table 2) was obtained from the AE-related information, and the variation law is shown in Figure 12(a). A gradual increase of initial pressure is observed with an increase of both slotting deviation angle and horizontal stress difference coefficient. Figure 12(b) presents a summary of the primary initial pressure statistics obtained by the DHF experiments. The numerical results are in good agreement with the experimental data. However, initiation pressures calculated by numerical analysis are slightly lower than the experimental values obtained under the same conditions. This difference can be explained by the pore pressure gradients that form in the three model slotting boreholes due to simultaneous injection with water. Following the theoretical analysis

Table 3: Numerical model and corresponding physical experiment number.

Number	Horizontal stress difference coefficient K_h	Slotting deviation angle θ (°)	Physical experiment number	Numerical model
1	0.5	30°	Sample 1	5#
2	0.5	45°	Sample 2	9#
3	0.5	60°	Sample 3	13#
4	0.5	90°	Sample 4	21#
5	0.75	45°	Sample 5	10#
6	1.0	45°	Sample 6	11#
7	1.25	45°	Sample 7	12#

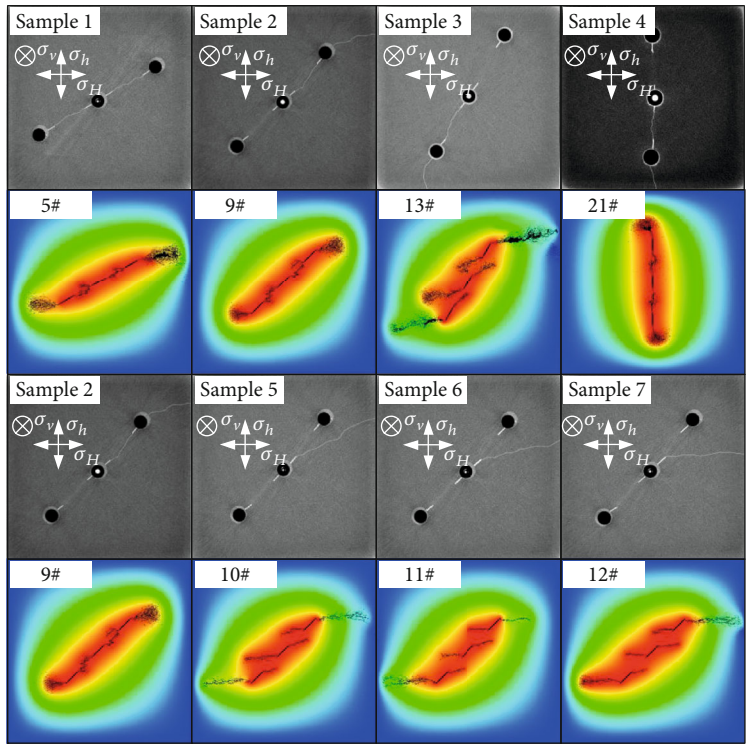

Figure 13: Comparison of crack propagation morphology between numerical calculations and physical experiments [18].

described in Section 2, a pore pressure gradient field can reduce the initial pressure, which explains the lower values derived from the model compared with the experiments.

Similarly, we compare crack propagation morphology obtained by numerical calculations with experimental results obtained under the same slotting deviation angle and horizontal stress difference coefficient. The corresponding relationship between physical experiments and numerical models is shown in Table 3.

Figure 13 shows CT images of the experimental cracks and numerical model crack propagation morphology. To study the influences of both preset slots and nonuniform pore pressure field on fracture propagation comprehensively, three slots were fractured simultaneously in the numerical model while only the center slot was fractured in previous physical experiments. Results obtained by the numerical calculation therefore provide more detailed insight into the crack propagation controlled process. In general, both datasets show similar crack propagation morphology and direction. The crack orientation propagation conditions summarized in Section 4.1 are therefore verified by the experimental results.

Even though the crack propagation morphology of physical experiments and numerical simulation have high similarities, they are not exactly the same for the existence of pore water pressure gradient. As the horizontal stress difference coefficient increases (samples 2, 5, 6, and 7), the cracks in the experiments gradually deflected towards the maximum horizontal principal stress, while cracks obtained by numerical simulation under identical conditions expand in the DHF inducing zone, even in the absence of direct connection. Therefore, the induced crack propagation effect is improved obviously upon the formation of a pore water pressure gradient.

5. Conclusion

Based on this study, the main conclusions can be drawn as follows:

(i) A novel method of DHF based on hydraulic slotting and a nonuniform pore pressure field is proposed in this paper. The hydraulic crack is oriented and extended using the two factors to disturb the local stress field of the rock. We have established a mechanical model of crack initiation and propagation by a nonuniform pore pressure field, which reveals the inducing effect of the nonuniform pore pressure field. The mechanical model shows that a pore water pressure gradient reduces the effective stress in the rock and that cracks tend to rupture and propagate towards higher pore pressure zones

(ii) Crack orientation propagation conditions are clarified. That is, when horizontal stress difference coefficients are less than or equal to 0.5 or the slotting deviation angle is less than or equal to 30°, the crack can achieve directional expansion. The smaller the slotting deviation angle and the horizontal stress difference coefficient, the better the directional effect of the DHF

(iii) The numerical results are verified by comparison with relevant experimental data. We compare and analyze the variation of crack initiation pressure and crack propagation morphology obtained from numerical analysis and physical experiments. Increased values of slotting deviation angle and/or horizontal stress difference coefficient lead to higher initial pressures, and a pore pressure gradient field can reduce the initial pressure. A comparison of the experimental and numerical results shows that the inducing effect improves in the presence of a pore pressure gradient field

Data Availability

The data used to support the findings of this study are available from the corresponding author upon request.

Conflicts of Interest

The authors declare that they have no conflicts of interest.

Acknowledgments

This study was supported by the National Natural Science Foundation of China (No. 51904049), the Natural Science Foundation of Chongqing (General Program, No. cstc2019jcyj-msxmX0702), the Chongqing Science and Technology Innovation Talent Support Program (No. CSTCCXLJRC201712), and the Chongqing basic science and frontier technology research project (cstc2017jcyj BX0076).

References

[1] H. C. Lau, H. Y. Li, and S. Huang, "Challenges and Opportunities of Coalbed Methane Development in China," *Energy & Fuels*, vol. 31, no. 5, pp. 4588–4602, 2017.

[2] Z. P. Meng, J. C. Zhang, and R. Wang, "In-situ stress, pore pressure and stress-dependent permeability in the Southern Qinshui Basin," *International Journal of Rock Mechanics and Mining Sciences*, vol. 48, no. 1, pp. 122–131, 2011.

[3] S. M. Liu and S. Harpalani, "Determination of the Effective Stress Law for Deformation in Coalbed Methane Reservoirs," *Rock Mechanics and Rock Engineering*, vol. 47, no. 5, pp. 1809–1820, 2014.

[4] B. X. Huang, Y. Z. Wang, and S. G. Cao, "Cavability control by hydraulic fracturing for top coal caving in hard thick coal seams," *International Journal of Rock Mechanics and Mining Sciences*, vol. 74, pp. 45–57, 2015.

[5] J. C. Zhang and X. B. Bian, "Numerical simulation of hydraulic fracturing coalbed methane reservoir with independent fracture grid," *Fuel*, vol. 143, pp. 543–546, 2015.

[6] Y. Y. Lu, F. Yang, Z. L. Ge, Q. Wang, and S. Q. Wang, "Influence of viscoelastic surfactant fracturing fluid on permeability of coal seams," *Fuel*, vol. 194, pp. 1–6, 2017.

[7] L. Zhou and M. Z. Hou, "A new numerical 3D-model for simulation of hydraulic fracturing in consideration of hydro-mechanical coupling effects," *International Journal of Rock Mechanics and Mining Sciences*, vol. 60, pp. 370–380, 2013.

[8] F. Hamidi and A. Mortazavi, "A new three dimensional approach to numerically model hydraulic fracturing process," *Journal of Petroleum Science and Engineering*, vol. 124, pp. 451–467, 2014.

[9] X. Sun, S. Zhang, X. Ma, Y. Zou, and G. Lin, "Experimental Investigation on Propagation Behavior of Hydraulic Fractures in Coal Seam during Refracturing," *Geofluids*, vol. 2019, Article ID 4278543, 15 pages, 2019.

[10] Q. Y. He, F. T. Suorineni, T. H. Ma, and J. Oh, "Effect of discontinuity stress shadows on hydraulic fracture re-orientation," *International Journal of Rock Mechanics and Mining Sciences*, vol. 91, pp. 179–194, 2017.

[11] D. Q. Li, S. Zhang, and S. A. Zhang, "Experimental and numerical simulation study on fracturing through interlayer to coal seam," *Journal of Natural Gas Science and Engineering*, vol. 21, pp. 386–396, 2014.

[12] Y. Liu, B. W. Xia, and X. T. Liu, "A novel method of orienting hydraulic fractures in coal mines and its mechanism of intensified conduction," *Journal of Natural Gas Science and Engineering*, vol. 27, pp. 190–199, 2015.

[13] X. Fu, G. S. Li, Z. W. Huang, Y. S. Liang, Z. M. Xu, and X. Jin, "Experimental and numerical study of radial lateral fracturing for coalbed methane," *Journal of Geophysics and Engineering*, vol. 12, no. 5, pp. 875–886, 2015.

[14] C. Lin, J. Q. Deng, Y. R. Liu, Q. Yang, and H. F. Duan, "Experiment simulation of hydraulic fracture in colliery hard roof control," *Journal of Petroleum Science and Engineering*, vol. 138, pp. 265–271, 2016.

[15] B. Yu, R. Gao, T. J. Kuang, B. J. Huo, and X. B. Meng, "Engineering study on fracturing high-level hard rock strata by ground hydraulic action," *Tunnelling and Underground Space Technology*, vol. 86, pp. 156–164, 2019.

[16] Y. J. Wang, J. Yang, M. C. He et al., "Test of a liquid directional roof-cutting technology for pressure-relief entry retaining

mining," *Journal of Geophysics and Engineering*, vol. 16, no. 3, pp. 620–638, 2019.

[17] Z. Ge, J. Zhong, Y. Lu et al., "Directional distance prediction model of slotting–directional hydraulic fracturing (SDHF) for coalbed methane (CBM) extraction," *Journal of Petroleum Science and Engineering*, vol. 183, article 106429, 2019.

[18] Y. G. Cheng, Y. Y. Lu, Z. L. Ge, L. Cheng, J. W. Zheng, and W. F. Zhang, "Experimental study on crack propagation control and mechanism analysis of directional hydraulic fracturing," *Fuel*, vol. 218, pp. 316–324, 2018.

[19] W. Lu, Y. Wang, and X. Zhang, "Numerical Simulation on the Basic Rules of Multihole Linear Codirectional Hydraulic Fracturing," *Geofluids*, vol. 2020, Article ID 6497368, 14 pages, 2020.

[20] F. Gao, Y. Xue, Y. A. Gao, Z. Z. Zhang, T. Teng, and X. Liang, "Fully coupled thermo-hydro-mechanical model for extraction of coal seam gas with slotted boreholes," *Journal of Natural Gas Science and Engineering*, vol. 31, pp. 226–235, 2016.

[21] H. He, L. M. Dou, J. Fan, T. T. Du, and X. L. Sun, "Deep-hole directional fracturing of thick hard roof for rockburst prevention," *Tunnelling and Underground Space Technology*, vol. 32, pp. 34–43, 2012.

[22] F. Z. Yan, B. Q. Lin, C. J. Zhu et al., "A novel ECBM extraction technology based on the integration of hydraulic slotting and hydraulic fracturing," *Journal of Natural Gas Science and Engineering*, vol. 22, pp. 571–579, 2015.

[23] C. Zhai, M. Li, C. Sun, J. G. Zhang, W. Yang, and Q. G. Li, "Guiding-controlling technology of coal seam hydraulic fracturing fractures extension," *International Journal of Mining Science and Technology*, vol. 22, no. 6, pp. 831–836, 2012.

[24] Y. Mizuta, S. Kikuchi, and K. Tokunaga, "Studies on hydraulic fracturing stress measurement assisted by water jet borehole slotting," *International Journal of Rock Mechanics and Mining Sciences & Geomechanics Abstracts*, vol. 30, no. 7, pp. 981–984, 1993.

[25] D. S. Zhou, P. Zheng, P. He, and J. Peng, "Hydraulic fracture propagation direction during volume fracturing in unconventional reservoirs," *Journal of Petroleum Science and Engineering*, vol. 141, pp. 82–89, 2016.

[26] R. B. Mao, Z. J. Feng, Z. H. Liu, and Y. S. Zhao, "Laboratory hydraulic fracturing test on large-scale pre-cracked granite specimens," *Journal of Natural Gas Science and Engineering*, vol. 44, pp. 278–286, 2017.

[27] J. Q. Deng, C. Lin, Q. Yang, Y. R. Liu, Z. F. Tao, and H. F. Duan, "Investigation of directional hydraulic fracturing based on true tri-axial experiment and finite element modeling," *Computers and Geotechnics*, vol. 75, pp. 28–47, 2016.

[28] T. Liu, B. Q. Lin, W. Yang, Q. L. Zou, J. Kong, and F. Z. Yan, "Cracking Process and Stress Field Evolution in Specimen Containing Combined Flaw Under Uniaxial Compression," *Rock Mechanics and Rock Engineering*, vol. 49, no. 8, pp. 3095–3113, 2016.

[29] T. Liu, B. Q. Lin, Q. L. Zou, C. J. Zhu, C. Guo, and J. Li, "Investigation on mechanical properties and damage evolution of coal after hydraulic slotting," *Journal of Natural Gas Science and Engineering*, vol. 24, pp. 489–499, 2015.

[30] M. S. Bruno and F. M. Nakagawa, "Pore pressure influence on tensile fracture propagation in sedimentary rock," *International Journal of Rock Mechanics and Mining Sciences & Geomechanics Abstracts*, vol. 28, no. 4, pp. 261–273, 1991.

[31] M. J. AlTammar, M. M. Sharma, and R. Manchanda, "The Effect of Pore Pressure on Hydraulic Fracture Growth: An Experimental Study," *Rock Mechanics and Rock Engineering*, vol. 51, no. 9, pp. 2709–2732, 2018.

[32] J. S. Huang, D. V. Griffiths, and S. W. Wong, "Initiation pressure, location and orientation of hydraulic fracture," *International Journal of Rock Mechanics and Mining Sciences*, vol. 49, pp. 59–67, 2012.

[33] J. S. Huang, D. V. Griffiths, and S. W. Wong, "In situ stress determination from inversion of hydraulic fracturing data," *International Journal of Rock Mechanics and Mining Sciences*, vol. 48, no. 3, pp. 476–481, 2011.

[34] M. M. Hossain, M. K. Rahman, and S. S. Rahman, "Hydraulic fracture initiation and propagation: roles of wellbore trajectory, perforation and stress regimes," *Journal of Petroleum Science and Engineering*, vol. 27, no. 3-4, pp. 129–149, 2000.

[35] Y. Y. Lu, L. Cheng, Z. L. Ge, B. W. Xia, Q. Li, and J. F. Chen, "Analysis on the Initial Cracking Parameters of Cross-Measure Hydraulic Fracture in Underground Coal Mines," *Energies*, vol. 8, no. 7, pp. 6977–6994, 2015.

[36] L. C. Li, C. A. Tang, and Y. F. Fu, "Influence of heterogeneity on fracture behavior in multi-layered materials subjected to thermo-mechanical loading," *Computational Materials Science*, vol. 46, no. 3, pp. 667–671, 2009.

[37] C. A. Tang, L. G. Tham, P. K. K. Lee, T. H. Yang, and L. C. Li, "Coupled analysis of flow, stress and damage (FSD) in rock failure," *International Journal of Rock Mechanics and Mining Sciences*, vol. 39, no. 4, pp. 477–489, 2002.

[38] B. G. da Silva and H. H. Einstein, "Finite Element study of fracture initiation in flaws subject to internal fluid pressure and vertical stress," *International Journal of Solids and Structures*, vol. 51, no. 23-24, pp. 4122–4136, 2014.